ROYAL SOCIETY
OF CHEMISTRY

PAPER

Check for updates

Ion density-enhanced electrostatic precipitation using high voltage nanosecond pulses†

Boxin Zhang,[d] Indu Aravind,[a] Sisi Yang,[a] Sizhe Weng,[c] Bofan Zhao,[c] Grace Johnson,[ef] Lucas Brown, [iD][ef] Jason Olfert, [iD][g] Heejung Jung [iD][ef] and Stephen B. Cronin [iD] ⋆[abc]

This study evaluates the beneficial effects of discharging nanosecond pulse transient plasma (NPTP) in a coaxial electrostatic precipitator for capturing nanoscale soot particles (∼50 nm) produced by an ethylene flame. Here, the nanoscale soot particles are collected using two different reactor geometries: a 3″ diameter reactor with a mean flow velocity of 1.2 m s^{-1} and a 1.5″ diameter reactor with a mean flow velocity 1.5 m s^{-1}, corresponding to volumetric flow rates of 11.5 CFM and 3.6 CFM, respectively. The nanosecond high voltage pulses (+20 kV, 20 ns, 800 Hz) are applied in conjunction with DC bias voltages. While nearly 100% collection efficiency can be achieved without NPTP at sufficiently high DC voltages ($|V_{DC}| > 14$ kV), this drops below 50% for lower DC voltages ($|V_{DC}| < 10$ kV). With NPTP, we observe substantially enhanced remediation (up to 23×) at lower DC voltages ($|V_{DC}| < 10$ kV) due to the enhanced ion density produced by the plasma. For DC-only electrostatic precipitation, the charging of soot particles takes place *via* a DC corona, whose ion density is several orders of magnitude lower than that of the NPTP, which produces a streamer discharge due to the fast rise times of the nanosecond pulses (*i.e.*, $dV/dt \sim 10^{12}$ V s^{-1}). High speed imaging of the plasma emission profile indicates that ion densities 10^6 times higher are achieved with the nanosecond pulsed plasma, as compared to that of the DC corona. At lower DC voltages (*i.e.*, $|V_{DC}| < 10$ kV), the charging of soot particles is a key factor limiting the DC-only remediation efficiencies, and NPTP provides a way to mitigate this limitation.

Environmental significance

The remediation of combustion generated particles (*i.e.*, soot or black carbon) produced by internal combustion engines is important due to their adverse health effects and their effects on climate change. There are currently no after treatment systems for controlling particulate emissions from medium and large ship engines. These ships emit soot at and near port, as well as in the open ocean, resulting in poor air quality near port areas and global climate change. We are reporting up to 23× enhancement in the collection efficiency (% remediation) of soot particles with nanosecond pulse transient plasma over a wide range of DC bias voltages from −15 kV to +15 kV. In the midst of accelerating climate change and global warming, our work in this field adds a significant scientific contribution to the ever-demanding search for cleaner automobile and industrial emissions.

1. Introduction

The remediation of combustion generated particles (*i.e.*, soot or black carbon) produced by internal combustion engines is

[a]Department of Physics and Astronomy, Los Angeles, CA 90089, USA. E-mail: scronin@usc.edu

[b]Department of Chemistry, Los Angeles, CA 90089, USA

[c]Ming Hsieh Department of Electrical Engineering, Los Angeles, CA 90089, USA

[d]Mork Family Department of Chemical Engineering and Materials Science, University of Southern California, Los Angeles, CA 90089, USA

[e]Department of Mechanical Engineering, Riverside, CA 92521, USA

[f]College of Engineering-Center for Environmental Research and Technology (CE-CERT), University of California, Riverside, Riverside, CA 92521, USA

[g]Department of Mechanical Engineering, University of Alberta, Edmonton, Alberta, Canada

important due to their adverse health effects and their effects on climate change.[1–3] Epidemiological studies show that fine particulates (*i.e.*, particles smaller than 2.5 μm) have been linked to lung cancer and premature cardiovascular, as well as respiratory deaths.[4–8] Predominantly produced by combustion, soot and black carbon were found to be the second major cause for global warming *via* direct solar absorption.[9] Particle emissions from on- and off-road vehicles and equipment can be controlled with diesel[10,11] or gasoline particulate filter[12] technologies. However, there are currently no after treatment systems for controlling particulate emissions from medium and large ship engines. These ships emit soot at and near port, as well as in the open ocean,[13–16] resulting in poor air quality near port areas and global climate change.[17]

Electrostatic precipitators (ESPs) are widely used to treat large volumes of particle laden flow.[18] Most coal-fired power plants are equipped with ESPs to reduce emissions of

particulates called fly ash. ESPs generally require a very large footprint and path length, which can be problematic for mobile sources.[19] In conventional ESPs, a corona discharge produced at high DC voltages generates ions that charge particles in the exhaust stream.[20] These charged particles are then swept out to the collecting electrodes by the electrostatic force of the DC voltage, thus, precipitating the particles out of the gas phase.[21] ESPs have not been adopted to remove diesel particulates from on-road diesel engines, as they require a long path and large device sizes to achieve a high enough collection efficiency.[22] While DC coronas in conventional ESPs are very effective in charging large particulates (*i.e.*, larger than 1 μm), they do a relatively poor job of charging sub-micron sized particles (*e.g.*, diesel particulates are typically ~100 nm).[23] Also, ESPs are not appropriate for treating dynamically changing exhaust emissions, such as diesel exhaust emissions for on-road vehicles. However, this limitation can be overcome if higher concentrations of ions can be generated. In a conventional ESP, a constant voltage is used to charge the particles (*via* corona discharge) and provide the electrostatic force needed to sweep them out to the collecting electrode. This DC corona discharge is inherently unstable, as the ionization threshold and arcing limit are often very close, leaving a narrow range of operation. At high enough voltages, dielectric breakdown occurs, resulting in the formation of a highly conducting arc (see Fig. S1 in the ESI†), which causes the electrostatic field between the two electrodes to collapse, terminating the electrostatic precipitation process. The arcing threshold (*i.e.*, dielectric breakdown) depends strongly on temperature,[24] which is particularly problematic for dynamically changing exhaust emissions that can be inhomogeneously distributed along the reactor length. Nanosecond high voltage pulses provide a way around this arcing threshold, enabling substantially higher peak fields to be achieved without arcing. With higher ion concentrations, more compact ESPs can be designed to effectively capture sub-micron particles and provide increased stability over a wider range of operating conditions. As such, it is important to develop new strategies and systems that can avoid instabilities related to arcing.

In the work presented here, we report the effect of transient plasma discharge on the collection efficiency of electrostatic precipitation of soot particles over a wide range of applied DC voltages based on particle size distribution measurements. The particle effective density, with and without transient nanosecond pulse plasma, was also measured to determine the change in particle mass distribution. Lastly, high speed imaging of the plasma distribution profile was performed on the transient plasma and DC corona in order to compare their relative ion densities.

2. Material and methods

Fig. 1 shows a schematic diagram of the experimental setup in which soot particles are generated using a Santoro-type diffusion flame burner with an ethylene flow rate of 4.8 SCCM and an air flow rate of 90 SCFH (2.5×10^6 SCCM). Soot particles are sampled using a 1/2″ stainless steel tube with a 1 mm sampling port that touches the tip of the flame (similar to the work of Higgins *et al.*[25]). HEPA-filtered particle-free air dilutes the sampling air stream at atmospheric pressure, and an ejector pump pulls the sample flow into a mini dilution tunnel. Both processes are incorporated in the dilutor shown in Fig. 1. The dilution tunnel is maintained at atmospheric pressure with circumferential vents located downstream to discharge extra sample flow into the fume hood. Sample flow is taken 2 inches upstream from the outlet exit at the centerline of the dilution tunnel and transferred to a 3-foot-long cylindrical coaxial reactor with a 0.025″ diameter center electrode and 1.5″ or 3″ outer diameter. The gas flowing through the reactor is at room temperature. With these two reactor diameters, we measured volumetric flow rates of 3.6 CFM (10^5 SCCM) and 11.5 CFM (3.3×10^5 SCCM), and mean flow velocities of 1.5 m s^{-1} and 1.2 m s^{-1} (assuming a plug flow), respectively. A high voltage nanosecond pulse generator (Model 20X, Transient Plasma Systems, Inc.) and a high voltage DC power supply (Glassman, Inc.) are used in conjunction with each other to initiate the electrostatic precipitation process. In order to do this safely, a large inductor (low pass filter) is used to protect the input of the DC power supply, and a large capacitor (high pass filter) protects the input of the nanosecond pulse power supply, as illustrated in Fig. S2 of the ESI.† The peak pulse voltage was 20 kV with a pulse duration of 20–30 ns, as plotted in Fig. 1. The pulse repetition rate was 0.8 kHz. The powers of "NPTP only" and "DC only" are 80 W and 42 W, respectively, and the power of "NPTP + DC" is 122 W. High speed images of the plasma discharge were taken with a PiMax 3 intensified CCD camera (Princeton Instruments).

Particle aerodynamic number-size distributions are measured using a Dekati ELPI+ aerosol particle size spectrometer (Model 2E10-10) over a range from 6 nm to 10 μm. Particle mobility number-size distributions were measured with a TSI Scanning Mobility Particle Sizer (Model 308200), which consists of a differential mobility analyzer (DMA, TSI Model 3080) and a condensation particle counter (CPC, TSI Model 3750). The DMA was set to a resolution of 0.3 nm, and the range of the measurement is 9.65 to 421.7 nm. The collection efficiency is calculated as the ratio of the total particle concentration (number or mass) with the ESP on divided by the particle concentration with the ESP off. The number concentrations are determined by integrating the particle number distribution over the range of each instrument. The particles generated by the flame were less than 300 nm (in either mobility or aerodynamic diameter).

The mass concentration of the aerosol is found by converting the number-size distributions to mass-size distributions and integrating. The relationship between particle size and particle mass (often expressed as the 'effective density' as a function of mobility diameter) is measured using a DMA (TSI Model 3080), which classifies particles by electrical mobility, in series with a centrifugal particle mass analyzer (CPMA, Cambustion Ltd),[26] which classifies particles by their mass-to-charge ratio, and a CPC (TSI Model 3750), as shown in Fig. 1. Details of the DMA-CPMA-CPC system and the effective density measurements of the soot are discussed in detail in Section S1 of the ESI.†

© 2023 The Author(s). Published by the Royal Society of Chemistry
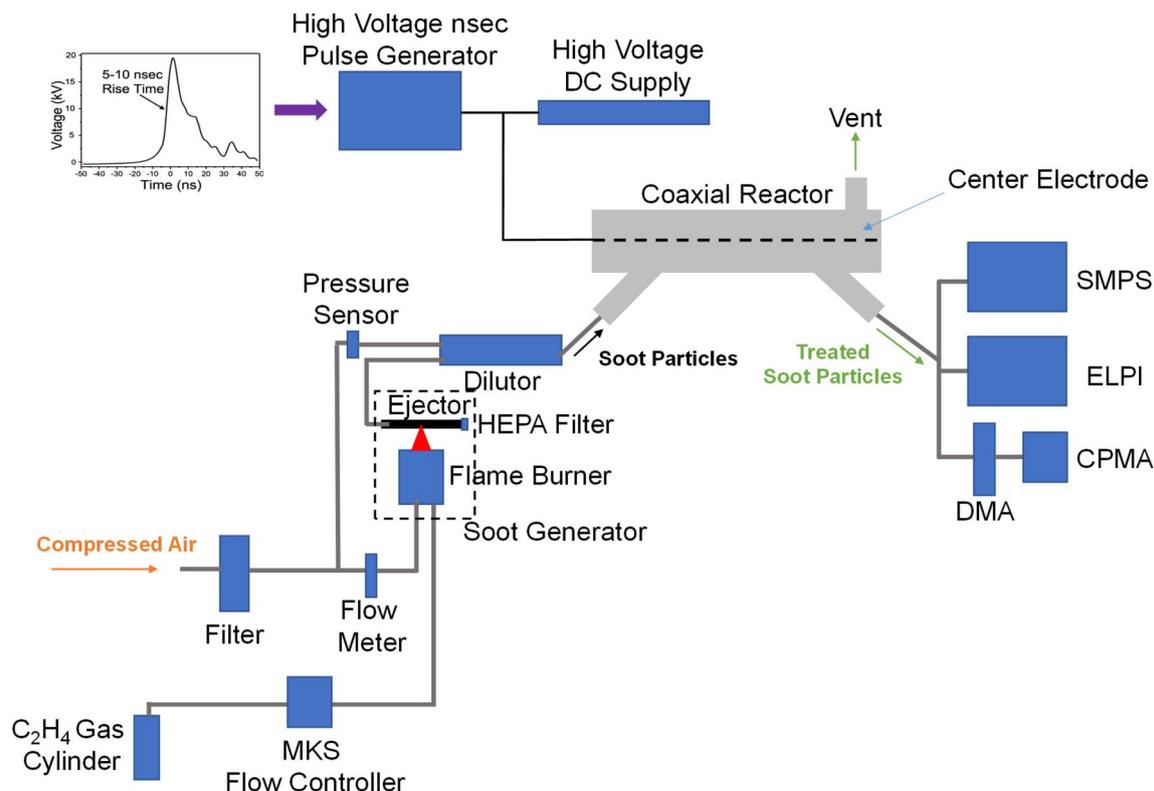
Environ. Sci.: Adv., 2023, **2**, 1566–1573 | **1567**

Fig. 1 Schematic diagram of the plasma-enhanced electrostatic precipitator (PE-ESP) soot remediation system and measurement configuration.

3. Results and discussion

To quantify the charge densities produced by the nanosecond pulse transient plasma (NPTP) discharge with respect to that of the DC corona, we performed time-resolved imaging of the NPTP produced as a function of the applied DC voltage. Fig. 2 shows high-speed images of the plasma discharge produced around the center wire electrode for the cases of DC only (Fig. 2a), NPTP only (Fig. 2b), and DC + NPTP (Fig. 2c). Here, the DC-only corona is produced locally near the surface of the center wire electrode. This DC-only image is multiplied by a factor of 1000 compared to those of Fig. 2b and c taken with the NPTP. It should be noted that these images were collected with a PiMax 3 intensified CCD camera (Princeton Instruments), which enables time-gating of the image collection. Here, images are collected over a relatively short window (100 μs) during each pulse event (repeated at 100 Hz). The camera is synchronized with (and delayed with respect to) the high voltage nanosecond pulses (100 Hz), as illustrated in Fig. S7 of the ESI.† The images were integrated over 100 cycles (*i.e.*, 10 s total measurement time, 0.01 s collection time (*i.e.*, exposure time)). These conditions were used for both "NPTP only" and "NPTP + DC". For "DC only" measurements, the gate width was also 100 μs but the frequency was 1 kHz, and the images were integrated over 100 000 cycles (*i.e.*, 100 s total measurement time, 10 s collection time). For the DC-only image, this corresponds to an exposure time that is 1000 times higher than the NPTP images, and is needed because of the relatively low light intensity

associated with the DC corona. For Fig. 2d, we integrated the intensity of all pixels, and the spatially extended transient plasma results in another factor of 1000× more luminescence than the DC corona, which is confined locally around the center electrode. The total emission intensity of the transient plasma (plotted in Fig. 2d) is more than 10^6 more luminescent than the DC corona during the first 500 ns after the high voltage pulse discharge. Fig. 2d shows a plot of the time evolution of the plasma emission intensity. Using this as a proxy for the charge density of the plasma, we find that the NPTP discharge produces more than 10^6 times higher plasma density than the DC corona, corroborating our previous assertion that the NPTP imparts more charge to the soot particles, thus, providing the basis for improved remediation.

Fig. 3a shows the particle number-based collection efficiency observed with the 1.5″-diameter reactor plotted as a function of DC voltage for DC-only and DC with nanosecond pulse transient plasma discharge using the ELPI+ particle spectrometer. Looking first at the DC-only data around zero bias voltage, we see the collection efficiency increasing monotonically under both positive and negative applied potentials, reaching around 40–50% remediation up to 10 kV for positive bias DC voltage and down to −9 kV for negative bias DC voltage. This low-bias remediation occurs because a fraction of the soot particles entering the reactor are already charged bipolar (*i.e.*, both positively and negatively charged particles) by chemical ions from the ethylene diffusion flame. Thus, for either negative or positive applied voltages, only half of the particles (*i.e.*, the
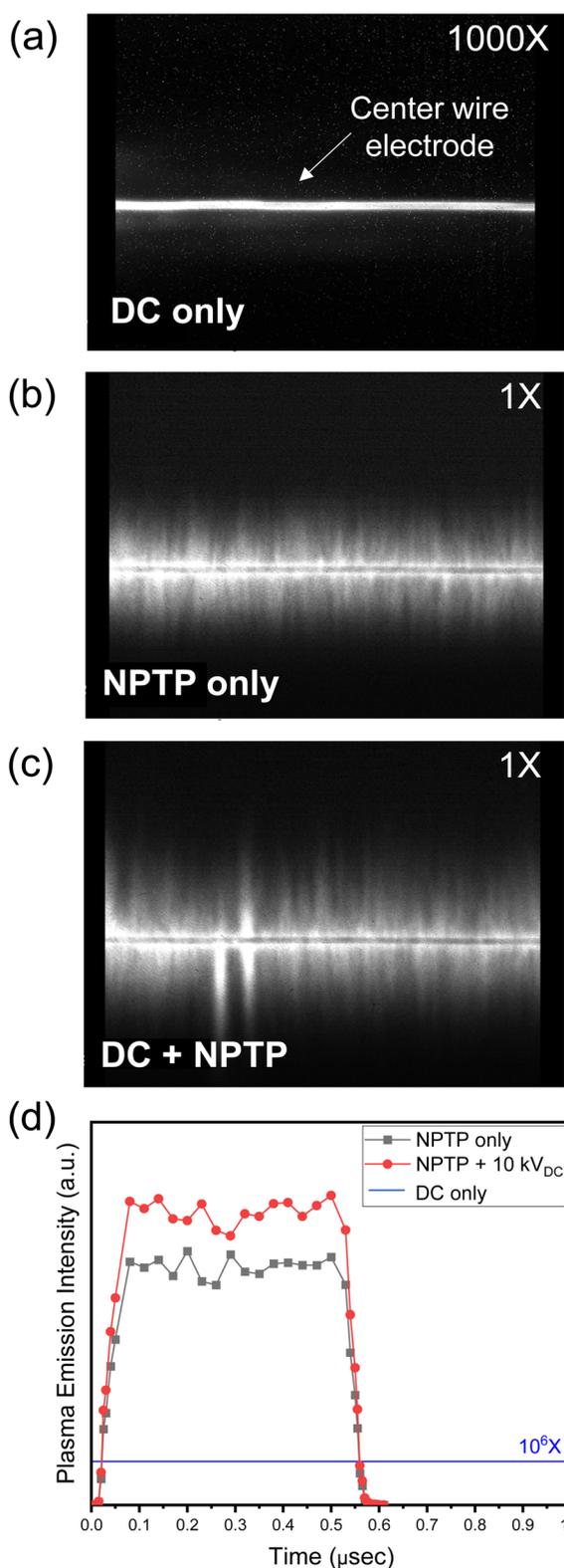
Fig. 2 CCD images of the center wire electrode for (a) DC only (17 kV), (b) NPTP only (0.8 kHz), and (c) NPTP (0.8 kHz) + DC (10 kV). (d) Time evolution of the intensity plots under different conditions (NPTP only, NPTP + 10 kV, and 17 kV DC only).
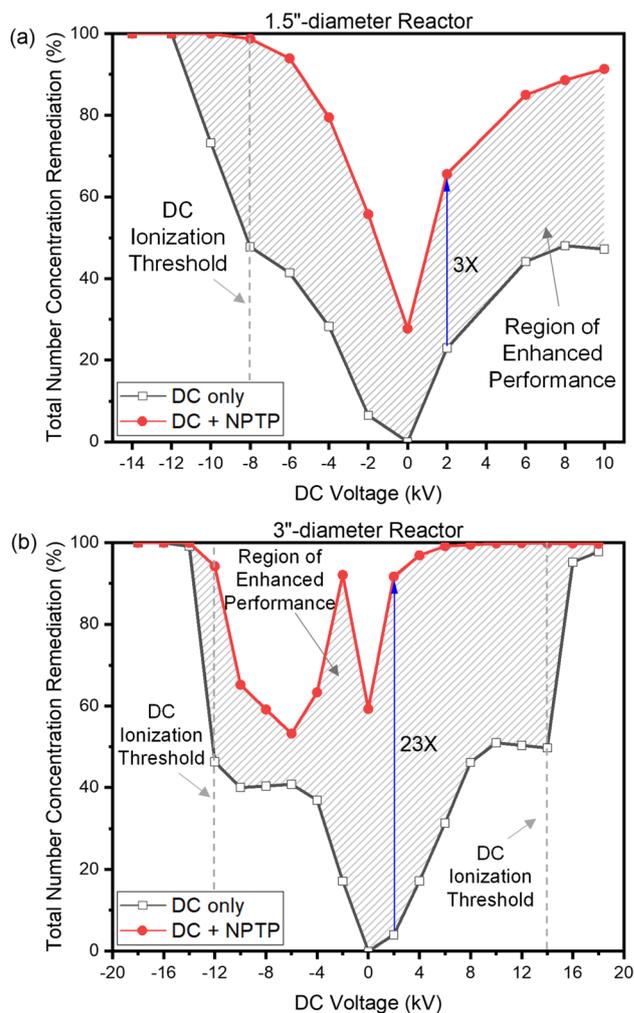

Fig. 3 Total particle number concentration remediation plots under DC only and DC + nanosecond pulse transient plasma (NPTP) at 0.8 kHz for (a) a 1.5″-diameter reactor and (b) a 3″-diameter reactor.

charged fraction) are remediated under DC-only conditions.[27] DC voltages $V_{DC} < -10$ kV lie above the threshold for ionization (*i.e.*, formation of a corona discharge), and the remediation rapidly jumps up to nearly 100% with increasing DC voltage as the DC corona discharge generates ions that impart charge to the soot particles. The data taken with transient plasma discharge (red data points) exhibit a roughly 2–3 fold enhancement in the remediation over the entire voltage range from −8 kV to +10 kV. This enhancement is due to the high concentrations of ions created by the high voltage nanosecond pulse discharges. High concentrations of both positive and negative ions may increase the average absolute charge per particle in both polarities, increasing particle electrical mobility. Originally, we had hoped that the plasma would oxidize/vaporize the soot particles. However, this does not appear to be the case, as evidenced by the poor remediation efficiency observed without the DC bias (*i.e.*, plasma only). Instead, the main effect of the plasma is to increase the ion

© 2023 The Author(s). Published by the Royal Society of Chemistry

Environ. Sci.: Adv., 2023, **2**, 1566–1573 | **1569**

density and, hence, charge per particle, thus, facilitating/enhancing the electrostatic precipitation process.

Fig. 3b shows the corresponding data taken with the 3′′-diameter reactor. Looking first at the DC-only data (black data points), we observe the same low-bias voltage dependence in which a fraction of soot particles is charged (imparted during combustion and subsequent soot formation process), resulting in a monotonically increasing dependence of the remediation on DC voltage that reaches a level of approximately 50% remediation. For high voltages $|V_{DC}| > 14$ kV that lie above the ionization threshold, the DC corona generates a substantial amount of charge, which is imparted to the soot particles
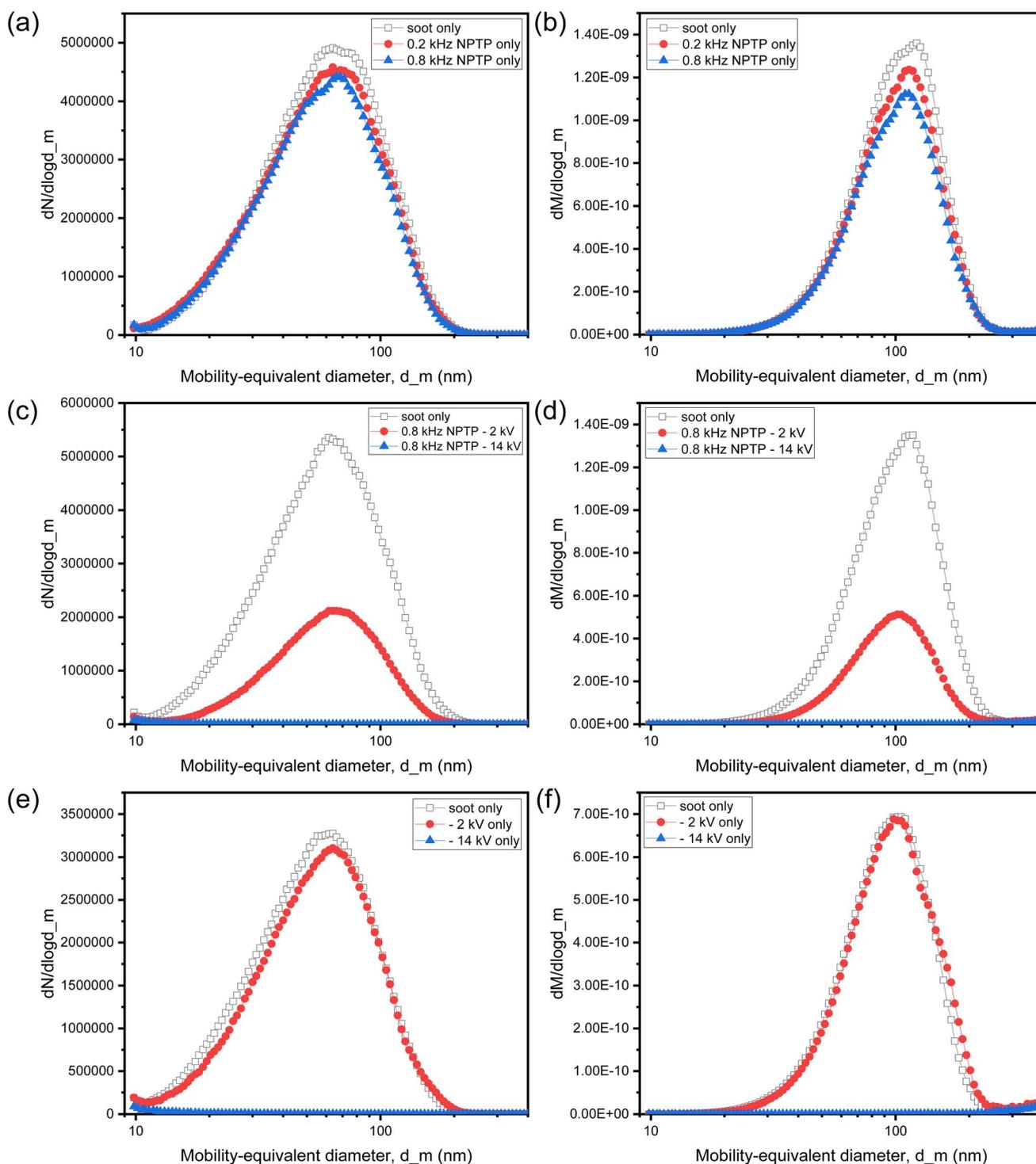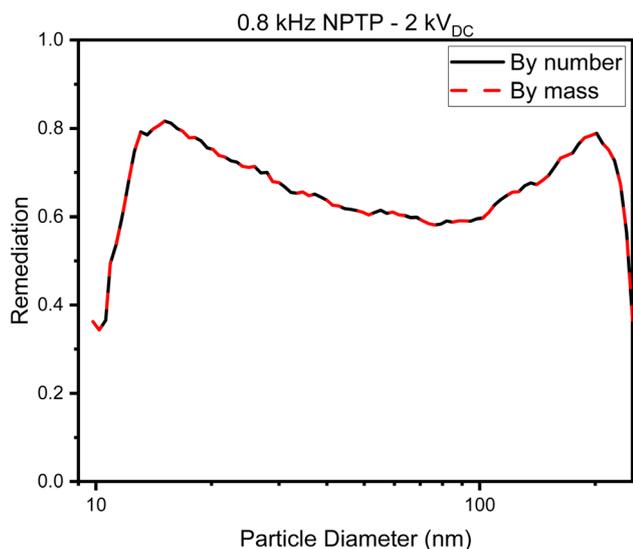

Fig. 4 Particle number (a), (c) and (e) and particle mass (b), (d) and (f) distributions measured under the following conditions: (a) and (b) NPTP only, (c) and (d) NPTP + negative V_{DC}, and (e) and (f) negative V_{DC} only.

Table 1 Calculated remediation efficiencies (%) from Fig. 4 data

	By number	By mass
0.2 kHz NPTP	6	11
0.8 kHz NPTP	12	18
0.8 kHz NPTP – 2 kV$_{DC}$	63	63
0.8 kHz NPTP – 14 kV$_{DC}$	100	100
−2 kV$_{DC}$	8	0
−14 kV$_{DC}$	99	99

Fig. 5 Plots of the particle remediation by number and by mass observed under 0.8 kHz NPTP − 2 kV$_{DC}$.

resulting in highly efficient electrostatic precipitation. The data taken with transient plasma discharge (red data points) again show a substantial enhancement in the remediation percentage over the entire voltage range from −12 kV to +14 kV. This enhancement is due to the large amount of charge generated by the high voltage nanosecond pulse plasma that imparts a large amount of charge to the soot particles, facilitating more efficient precipitation to the sidewalls of the reactor. There is, however, a slight drop in the plasma-enhanced remediation over the range from −4 kV to −8 kV due to the partial cancelation of the positive nanosecond pulse voltage by the negative applied DC voltage.

Fig. 4 compares the particle number and particle mass distributions under several test conditions measured using SMPS spectroscopy. The particle mass distributions were determined using the particle effective density (Fig. S3†) along with their number distribution. The particle number mean diameter is centered around 60 nm for all cases, while the particle mass mean diameter is centered around 120 nm. Table 1 summarizes the remediation efficiencies by number and mass obtained by integrating the distributions plotted in Fig. 4. The particle effective density with pulser on was used for −14 kV$_{DC}$ because of the expected ozone production due to the corona discharge, while the baseline particle effective density was used

for −2 kV$_{DC}$ due to the absence of corona discharge and corresponding absence of ozone. It is well known that ozone is produced by the plasma, however, for engine exhaust ozone is consumed rapidly by NO. As such, we typically do not observe any ozone in real exhaust applications. The remediation efficiencies obtained by mass and number were in close agreement with each other except in two cases: 0.2 kHz pulser only and −2 kV$_{DC}$ only. The size-dependent, number-based remediation efficiencies obtained under 0.8 kHz pulse frequency and 2 kV$_{DC}$ bias conditions are plotted in Fig. 5. The collection efficiency profile from 16 nm to 200 nm exhibits a diameter dependence similar to a previous study showing minima around 75 nm.[29] In this previous work, Ehara *et al.* explained the decrease in collection efficiency by re-entrainment of particles. However, the authors do not fully understand the sharp decrease in collection efficiency below 16 nm and indicate that further investigation is necessary. The diameter dependence of the remediation obtained with the ELPI particle size spectrometer are plotted in Fig. S4–S6 of the ESI.†

Our previous work[28] reported the use of plasma-enhanced electrostatic precipitation in diesel engine exhaust under engine relevant conditions. In the work presented here, we perform high speed optical imaging of the transient plasma, DC corona, and transient plasma + DC bias. This optical study demonstrates ion density enhancement *via* transient plasma and provides a way to explain the large increase in the collection efficiency of soot particles at low V_{DC} with plasma. We also investigate a wide range of V_{DC} (*i.e.*, −18 kV to +18 kV) for a full dataset of collection efficiency at various V_{DC} with and without plasma, whereas our previous paper only studied a few DC voltages. In particular, this study provides an important comparison of the NPTP under positive and negative applied bias voltages. Lastly, the soot particles used in this study were produced by a flame burner rather than a diesel engine, which eliminates several effects associated with moisture, NO and high temperatures.

4.   Conclusions

In conclusion, we have demonstrated enhanced electrostatic precipitation of nanoscale soot particles produced in the combustion of hydrocarbon fuel (ethylene) by discharging nanosecond pulse transient plasma (NPTP) in conjunction with a DC bias voltage. The collection efficiency (% remediation) increases by as much as 23-fold with NPTP discharge, and enhancement is observed over a wide range of DC bias voltages from −15 kV to +15 kV. This plasma-enhanced approach (*i.e.*, plasma-enhanced electrostatic precipitation) provides a way to eliminate the instabilities in the conventional (DC-only) electrostatic precipitation process associated with the DC corona ionization and arcing by using NPTP. Time-resolved images of the center wire electrode enable a relative measure of the plasma densities, showing that the NPTP discharge produces more than 10^6 times higher plasma density than the DC corona, corroborating our previous assertion that the NPTP simply imparts more charge to the soot particles, thus, forming the basis for the improved remediation.

© 2023 The Author(s). Published by the Royal Society of Chemistry

Environ. Sci.: Adv., 2023, **2**, 1566–1573 | **1571**

Conflicts of interest

There are no conflicts to declare.

Acknowledgements

References

1 I. M. Kennedy, The health effects of combustion-generated aerosols, *Proc. Combust. Inst.*, 2007, **31**(2), 2757–2770.

2 J. S. Lighty, J. M. Veranth and A. F. Sarofim, Combustion aerosols: factors governing their size and composition and implications to human health, *J. Air Waste Manage. Assoc.*, 2000, **50**(9), 1565–1618.

3 H. Burtscher, Physical characterization of particulate emissions from diesel engines: a review, *J. Aerosol Sci.*, 2005, **36**(7), 896–932.

4 G. Oberdörster, E. Oberdörster and J. Oberdörster, Nanotoxicology: an emerging discipline evolving from studies of ultrafine particles, *Environ. Health Perspect.*, 2005, **113**(7), 823–839.

5 J. C. Chow, J. G. Watson, J. L. Mauderly, D. L. Costa, R. E. Wyzga, S. Vedal, G. M. Hidy, S. L. Altshuler, D. Marrack and J. M. Heuss, Health effects of fine particulate air pollution: lines that connect, *J. Air Waste Manage. Assoc.*, 2006, **56**(10), 1368–1380.

6 C. A. Pope III, R. T. Burnett, M. J. Thun, E. E. Calle, D. Krewski, K. Ito and G. D. Thurston, Lung cancer, cardiopulmonary mortality, and long-term exposure to fine particulate air pollution, *JAMA*, 2002, **287**(9), 1132–1141.

7 J. M. Samet, F. Dominici, F. C. Curriero, I. Coursac and S. L. Zeger, Fine particulate air pollution and mortality in 20 US cities, 1987–1994, *N. Engl. J. Med.*, 2000, **343**(24), 1742–1749.

8 H. D. E. Panel, *Diesel emissions and lung cancer: an evaluation of recent epidemiological evidence for quantitative risk assessment*, Health Effects Institute, Boston, MA, 2015.

9 T. C. Bond, S. J. Doherty, D. W. Fahey, P. M. Forster, T. Berntsen, B. J. DeAngelo, M. G. Flanner, S. Ghan, B. Kärcher and D. Koch, Bounding the role of black carbon in the climate system: a scientific assessment, *J. Geophys. Res.: Atmos.*, 2013, **118**(11), 5380–5552.

10 B. A. Van Setten, M. Makkee and J. A. Moulijn, Science and technology of catalytic diesel particulate filters, *Catal. Rev.*, 2001, **43**(4), 489–564.

11 M. K. Khair, *A review of diesel particulate filter technologies*, 2003.

12 A. Joshi and T. V. Johnson, Gasoline particulate filters—a review, *Emiss. Control Sci. Technol.*, 2018, **4**(4), 219–239.

13 J. J. Corbett and P. Fischbeck, Emissions from ships, *Science*, 1997, **278**(5339), 823–824.

14 D. Cooper, Exhaust emissions from ships at berth, *Atmos. Environ.*, 2003, **37**(27), 3817–3830.

15 M. Tichavska, B. Tovar, D. Gritsenko, L. Johansson and J. P. Jalkanen, Air emissions from ships in port: does regulation make a difference?, *Transport Policy*, 2019, **75**, 128–140.

16 H. Winnes, L. Styhre and E. Fridell, Reducing GHG emissions from ships in port areas, *Research in Transportation Business & Management*, 2015, **17**, 73–82.

17 A. Mousavi, M. H. Sowlat, S. Hasheminassab, A. Polidori, M. M. Shafer, J. J. Schauer and C. Sioutas, Impact of emissions from the Ports of Los Angeles and Long Beach on the oxidative potential of ambient PM0.25 measured across the Los Angeles County, *Sci. Total Environ.*, 2019, **651**, 638–647.

18 K. R. Parker, Why an electrostatic precipitator?, in *Applied Electrostatic Precipitation*, Springer, 1997, pp. 1–10.

19 D. B. Kittelson, D. Y. Pui and K. Moon, Electrostatic collection of diesel particles, *SAE Trans.*, 1986, 51–62.

20 A. Jaworek, A. Marchewicz, A. Sobczyk, A. Krupa and T. Czech, Two-stage electrostatic precipitators for the reduction of PM2.5 particle emission, *Prog. Energy Combust. Sci.*, 2018, **67**, 206–233.

21 S. H. Lee, E. Sakai, M. Daimon and W. K. Bang, Characterization of fly ash directly collected from electrostatic precipitator, *Cem. Concr. Res.*, 1999, **29**(11), 1791–1797.

22 K. Parker, *Electrical operation of electrostatic precipitators*, IET, 2003.

23 D. Xu, J. Li, Y. Wu, L. Wang, D. Sun, Z. Liu and Y. Zhang, Discharge characteristics and applications for electrostatic precipitation of direct current: corona with spraying discharge electrodes, *J. Electrost.*, 2003, **57**(3–4), 217–224.

24 P. Yan, C. Zheng, G. Xiao, X. Xu, X. Gao, Z. Luo and K. Cen, Characteristics of negative DC corona discharge in a wire–plate configuration at high temperatures, *Sep. Purif. Technol.*, 2015, **139**, 5–13.

25 K. J. Higgins, H. Jung, D. B. Kittelson, J. T. Roberts and M. R. Zachariah, Size-selected nanoparticle chemistry: kinetics of soot oxidation, *J. Phys. Chem. A*, 2002, **106**(1), 96–103.

26 J. Olfert and N. Collings, New method for particle mass classification—the Couette centrifugal particle mass analyzer, *J. Aerosol Sci.*, 2005, **36**(11), 1338–1352.

27 S. Kim, K. Woo, B. Liu and M. Zachariah, Method of measuring charge distribution of nanosized aerosols, *J. Colloid Interface Sci.*, 2005, **282**(1), 46–57.

28 B. Zhang, I. Aravind, S. Yang, S. Weng, B. Zhao, C. Schroeder, W. Schroeder, M. Thomas, R. Umstattd and D. Singleton, Plasma-enhanced electrostatic precipitation of diesel exhaust particulates using nanosecond high voltage pulse discharge for mobile source emission control, *Sci. Total Environ.*, 2022, **851**, 158181.

29 Y. Ehara, A. Osako, A. Zukeran, K. Kawakami and T. Inui, Diesel PM collection for marine emission using hole-type electrostatic precipitators, *WIT Trans. Ecol. Environ.*, 2014, **183**, 145–155.

© 2023 The Author(s). Published by the Royal Society of Chemistry

Environ. Sci.: Adv., 2023, **2**, 1566–1573 | **1573**